SUPPORTING INFORMATION

Multifunctional Magnetic CuS/Gd_2O_3 Nanoparticles for Fluorescence/MR Bimodal Imaging-guided Photothermal-intensified Chemodynamic Synergetic Therapy of Targeted Tumors

Minchuan Luo[1], Hiroshi Yukawa[1,2,3,4,5]*, Kazuhide Sato[2,4,6], Makoto Tozawa[7], Masato Tokunaga[1], Tatsuya Kameyama[7], Tsukasa Torimoto[7] and Yoshinobu Baba[1,2,3]*

1. Nanobio Analytical Chemistry, Biomolecular Chemistry, Department of Biomolecular Engineering, Graduate School of Engineering, Nagoya University, Furo-cho, Chikusa-ku, Nagoya 464-8603, Japan

2. Institute of Nano-Life-Systems, Institutes of Innovation for Future Society, Nagoya University, Furo-cho, Chikusa-ku, Nagoya 464-8603, Japan

3. Institute of Quantum Life Science, Quantum Life and Medical Science Directorate, National Institutes for Quantum Science and Technology, Anagawa, Inageku, Chiba 263-8555, Japan

4. Nagoya University Institute for Advanced Research, Advanced Analytical and Diagnostic Imaging Center (AADIC)/Medical Engineering Unit (MEU), B3 Unit, Tsurumai 65, Showa-ku, Nagoya 466-8550, Japan

5. Development of Quantum-nano Cancer Photoimmunotherapy for Clinical Application of Refractory Cancer, Nagoya University, Tsurumai 65, Showa-ku, Nagoya 466-8550, Japan

6. Nagoya University Institute for Advanced Research, S-YLC, Furo-cho, Chikusa-ku, Nagoya 464-8603, Japan

7. Material Design Chemistry, Department of Materials Chemistry, Graduate School of Engineering, Nagoya University, Furo-cho, Chikusa-ku, Nagoya 464-8603, Japan

*Corresponding authors

E-mail: h.yukawa@nanobio.nagoya-u.ac.jp & babaymtt@chembio.nagoya-u.ac.jp

Tel: +81-52-789-5654, Fax: +81-52-789-5117

Table of Contents

SUPPLEMENTARY FIGURES

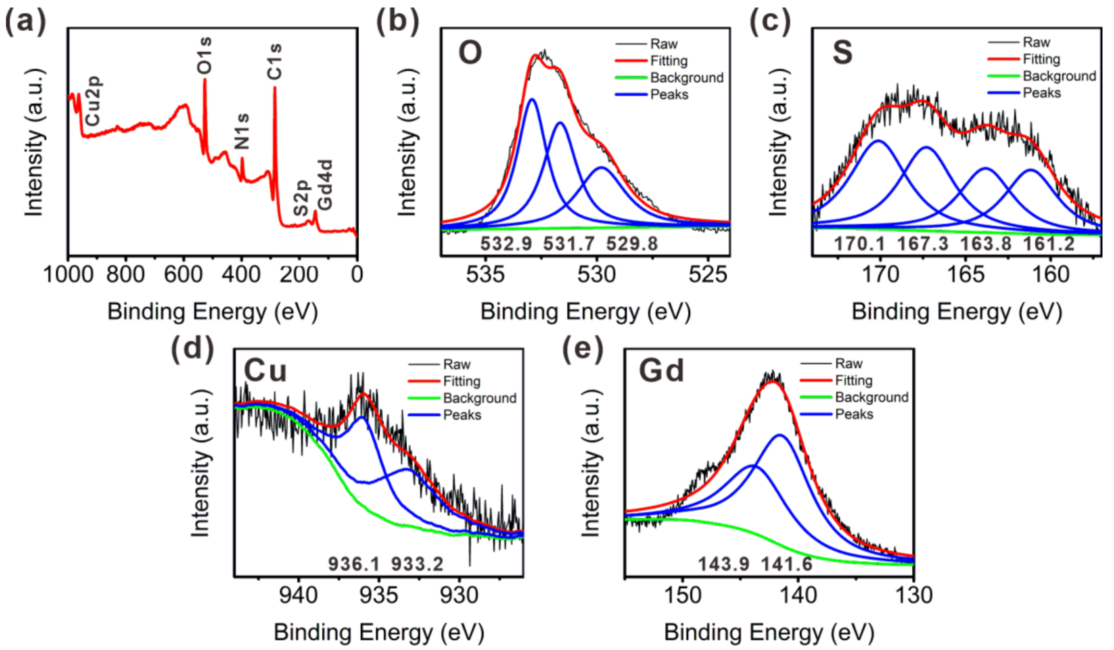

Figure S1. XPS spectra of BCG. (a) Original spectrum. (b) Characteristic peaks of O 1s (−COOH and −OH in BSA: 532.9 ev, $Gd(OH)_3$: 531.7 ev, Gd_2O_3: 529.8 ev). (c) Characteristic peaks of S 2p ($CuSO_4$: 170.1 ev and 167.3 ev, CuS: 163.8 ev and 161.2 ev). (d) Characteristic peaks of Cu 2p (CuS: 933.2 ev). (e) Characteristic peaks of Gd 4d (Gd_2O_3: 143.9 ev, $Gd(OH)_3$: 141.6 ev).[1, 2]

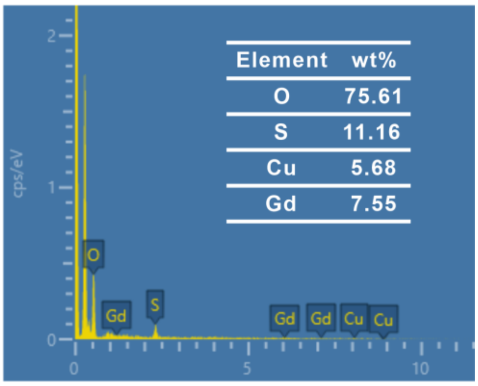

Figure S2. The EDS analysis of BCG and wt% for O, S, Cu and Gd elements.

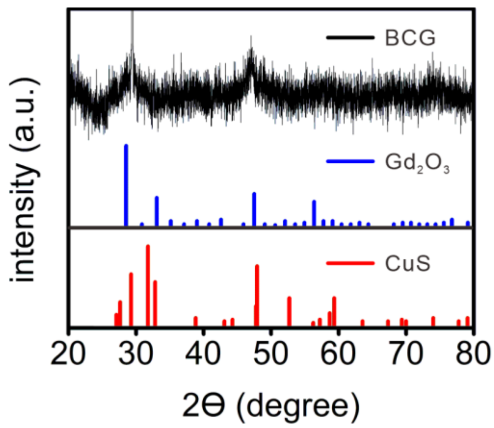

Figure S3. Powder XRD patterns of BCG, as referenced by the standard hexagonal CuS (JCPDS 06-0464) and cubic Gd_2O_3 (JCPDS 12-0797), in which 1/8 of the original mass of BSA was used to synthesize BCG to reduce the interference towards the signal of CuS and Gd_2O_3.

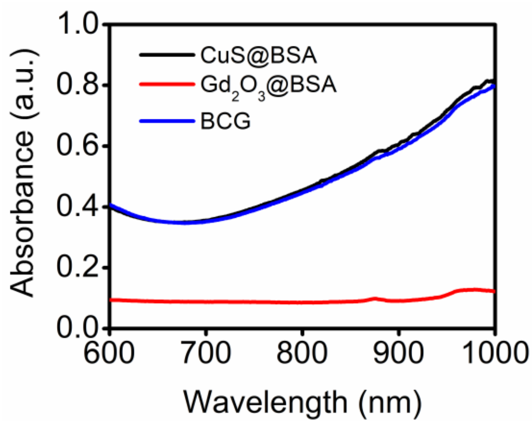

Figure S4. Absorption spectra of CuS capped by BSA, Gd_2O_3 capped by BSA and BCG (20 mg/mL) with similar synthesis conditions.

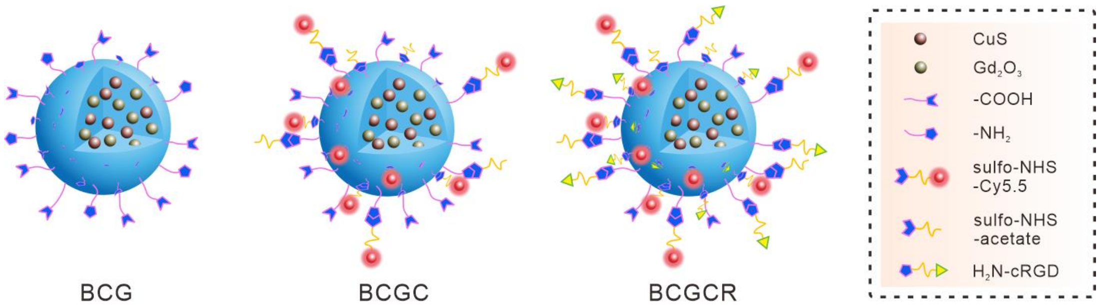

Figure S5. Cartoon diagrams of BSA-CuS-Gd_2O_3 (BCG), BSA-CuS-Gd_2O_3-Cy5.5 (BCGC) and BSA-CuS-Gd_2O_3-Cy5.5-RGD (BCGCR).

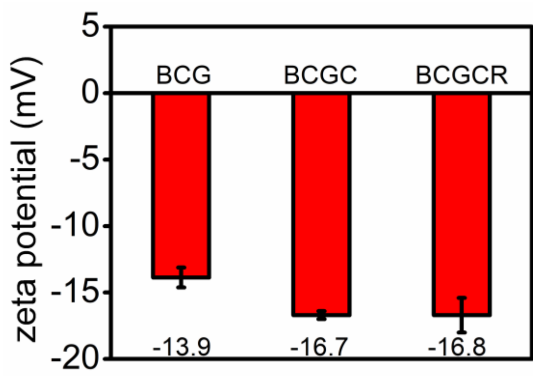

Figure S6. Zeta potentials of BCG, BCGC and BCGCR.

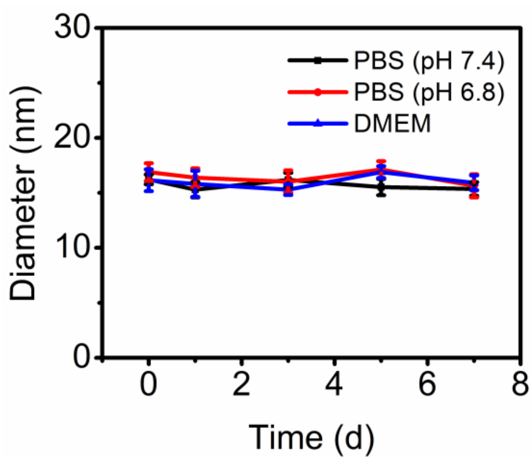

Figure S7. A long-term size investigation of BCGCR in PBS (pH 7.4), PBS (pH 6.8) and DMEM using a DLS analysis.

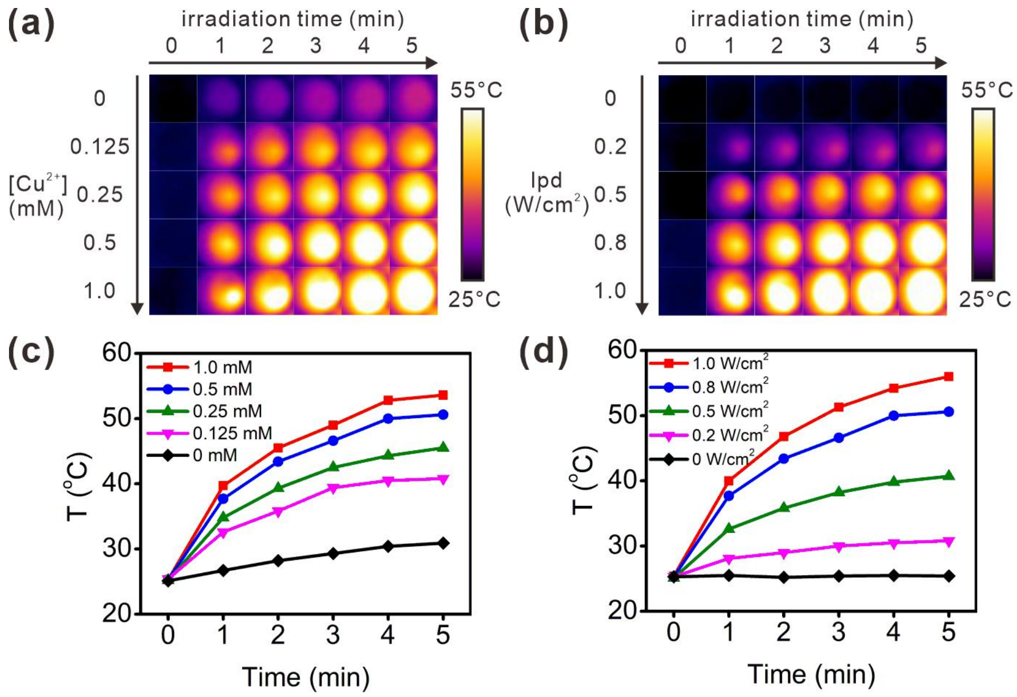

Figure S8. IR thermal images and average temperature variations of BCGCR solution under 980 nm laser irradiation for 5 min. (a & c) Different concentrations of BCGCR (0~1.0 mM Cu^{2+}) with a power density of 0.8 W/cm^2. (b & d) BCGCR (0.5 mM Cu^{2+}) with different laser power densities (lpd) (0~1 W/cm^2).

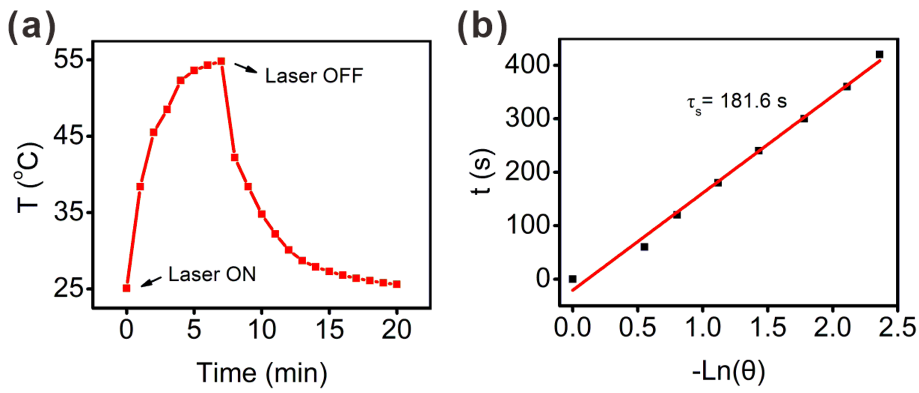

Figure S9. PCE evaluation of BCGCR. (a) Temperature variation of BCGCR solution (1 mM Cu^{2+}) under 980 nm laser irradiation (0.8 W/cm^2) for 7 min followed by natural cooling. (b) Measurement of the thermal time constant (τ_s) by linear fit of the time point t vs (- Lnθ) during the natural cooling period. The PCE was calculated as 30.3% according to Note S1.

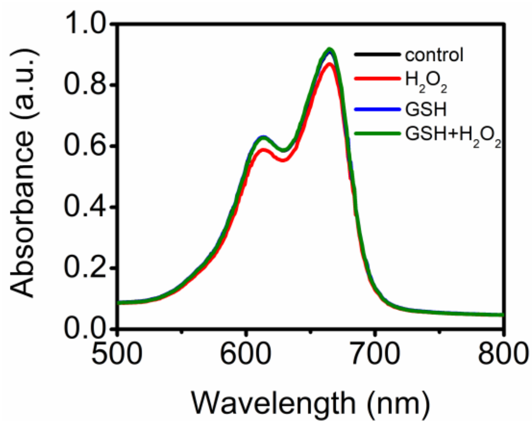

Figure S10. Absorption spectra of (10 μg/mL) MB with H_2O_2 (20 mM), GSH (1 mM) or H_2O_2 + GSH at pH 5.4 for 5 min.

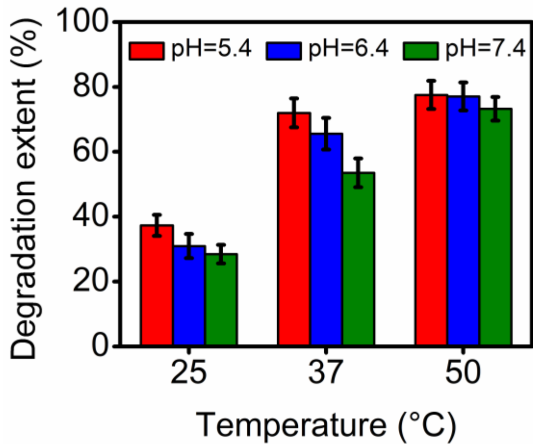

Figure S11. The extent of MB (10 μg/mL) degradation reflected by decreased absorbance after incubation with BCG-GSH (0.5 mM Cu^{2+}) and H_2O_2 (20 mM) at varying pH values and temperatures for 20 min.

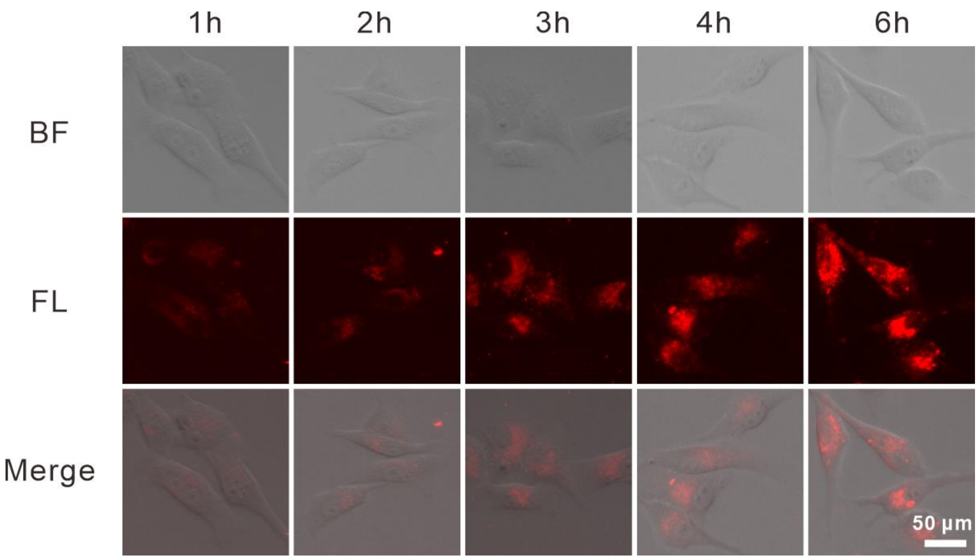

Figure S12. Fluorescence images of U87MG cells after incubation with BCGCR (100 μg/mL) for 1, 2, 3, 4, and 6 h.

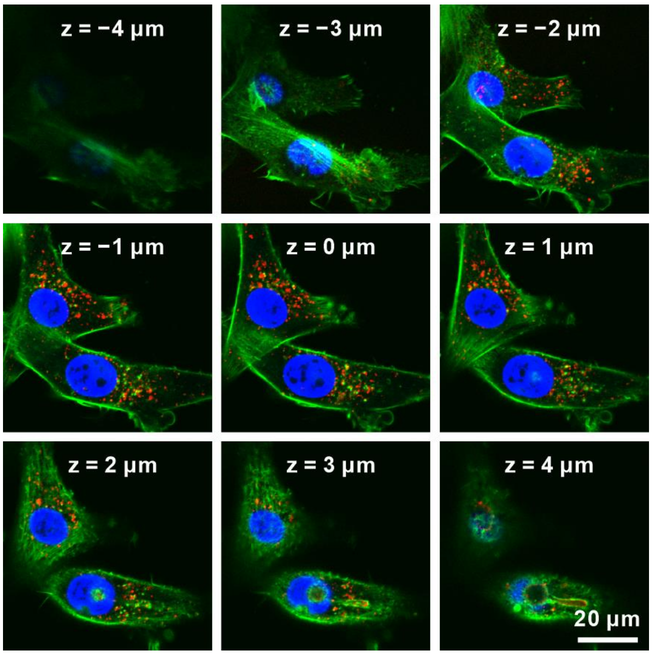

Figure S13. A set of confocal fluorescence images at different depths of U87MG cells incubated with BCGCR (50 μg/mL) (red) for 2 h, followed by co-staining with 0.1 μg/mL Hoechst 33342 (blue) and 300 nM Alexa Fluor™ 488 Phalloidin (green) for 30 min.

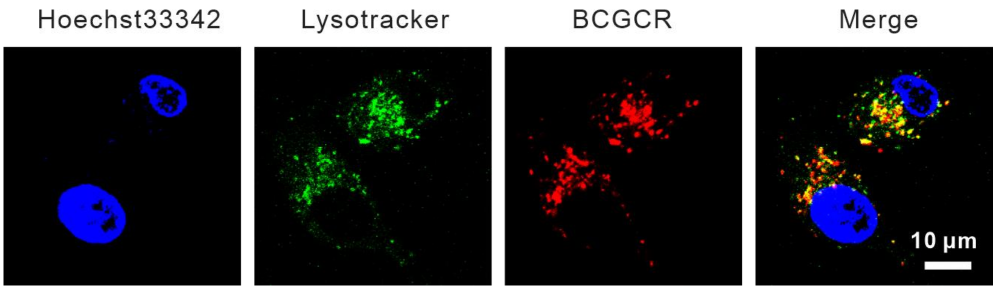

Figure S14. Colocalization study of U87MG cells after incubation with BCGCR (50 μg/mL) (red) for 2 h, followed by co-staining with 0.1 μg/mL Hoechst 33342 (blue) and 200 nM Lysotracker (green) for 20 min.

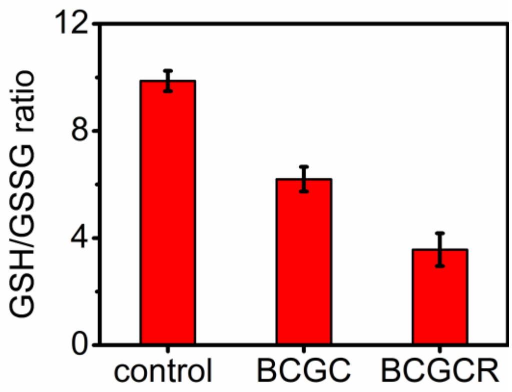

Figure S15. The GSH level in U87MG cells (untreated, incubated with 100 μg/mL BCGC or BCGCR, 6 h).

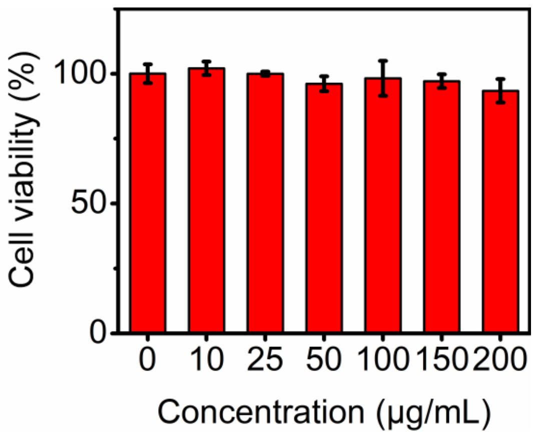

Figure S16. HEK293T cell viability after incubation with different concentrations of BCGCR for 24 h.

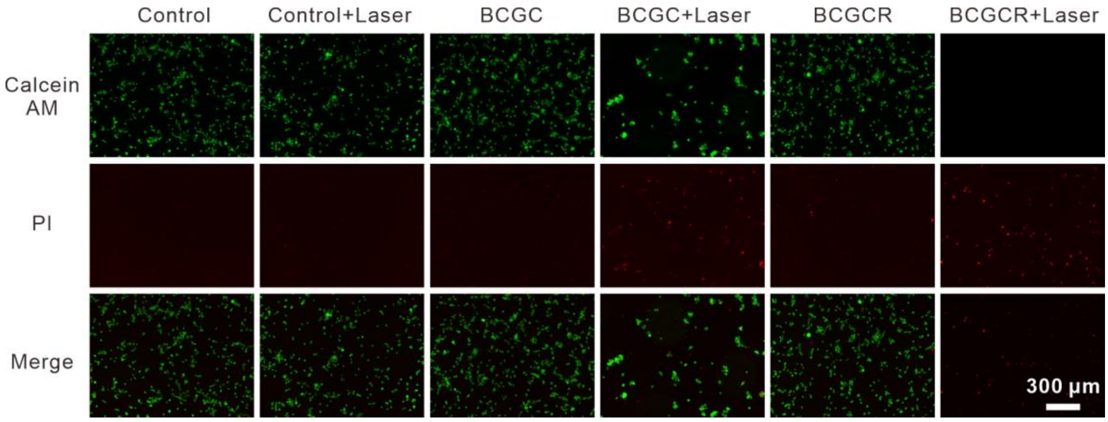

Figure S17. Fluorescence images of live (green) and dead (red) U87MG cells. Cells were incubated with BCGC or BCGCR (200 μg/mL) for 24 h followed by exposure under laser irradiation (or non-exposure) (980 nm, 0.8 W/cm^2) for 5 min, and stained with Calcein AM and PI for 30 min.

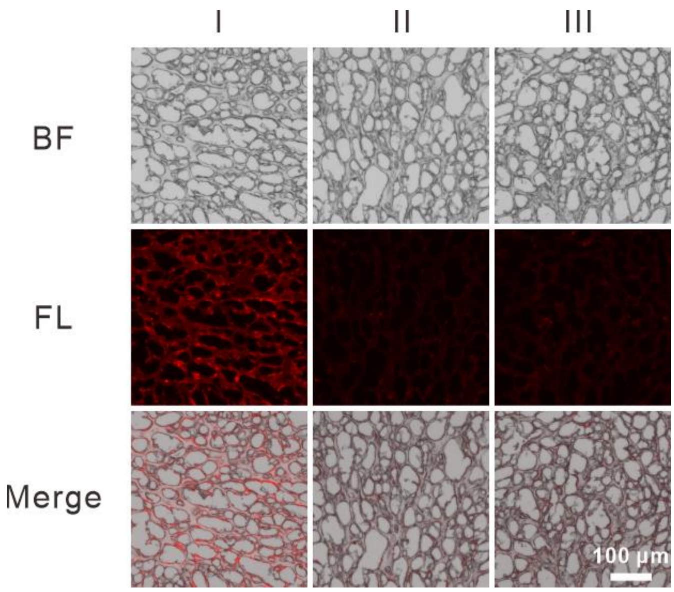

Figure S18. Fluorescence images of tumor tissue slices resected from U87MG tumor bearing mice at 2 days after (I) i.v. injection of BCGCR (5 mg/kg, 100 μL), (II) i.t. injection of free cRGDfk (2 mM, 100 μL) followed by i.v. injection of BCGCR (5 mg/kg, 100 μL) 1 h later, (III) i.v. injection of BCGC (5 mg/kg, 100 μL).

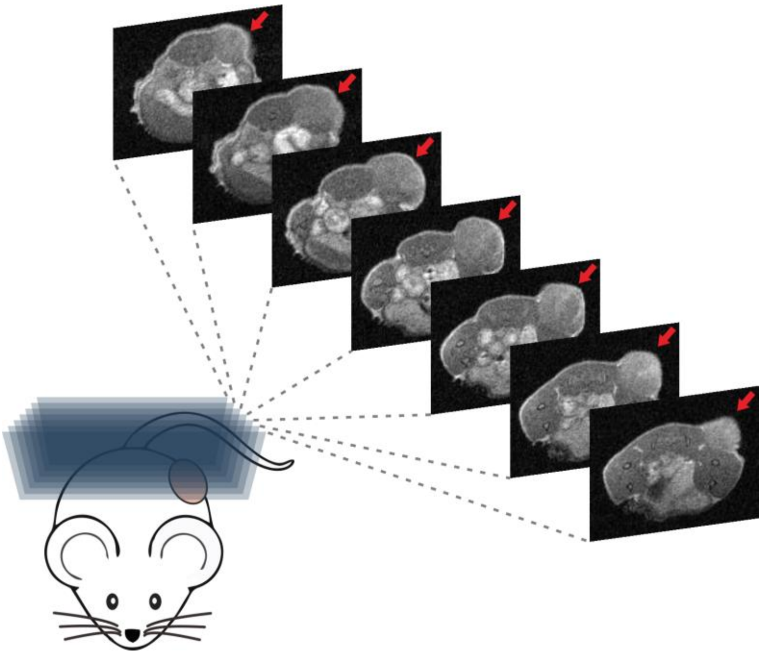

Figure S19. T_1-weighted multi-slice MR images of mice at 2 days after the i.v. injection of BCGCR (20 μmol/kg Gd^{3+}, 200 μL) (TR/TE = 500/9.0 ms at 1.5 T). Red arrows indicate tumor locations in mice.

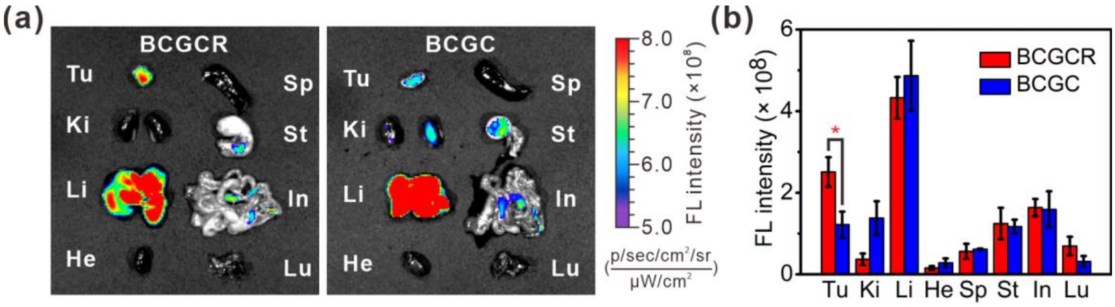

Figure S20. Study of fluorescence distribution in U87MG tumors and main organs. (a) Fluorescence images of tumors and main organs resected from mice at 2 days after i.v. injection of BCGC or BCGCR (2 mg/kg, 50 μL) (Ex: 675 nm, Em: 720 nm). Tu: tumor; Ki: kidneys; Li: liver; He: heart; Sp: spleen; St: stomach; In: intestines; Lu: lungs. (b) Statistics of average FL intensity of tumors and main organs in (a). Values denote the mean ± SD (n = 3, $^*P < 0.05$).

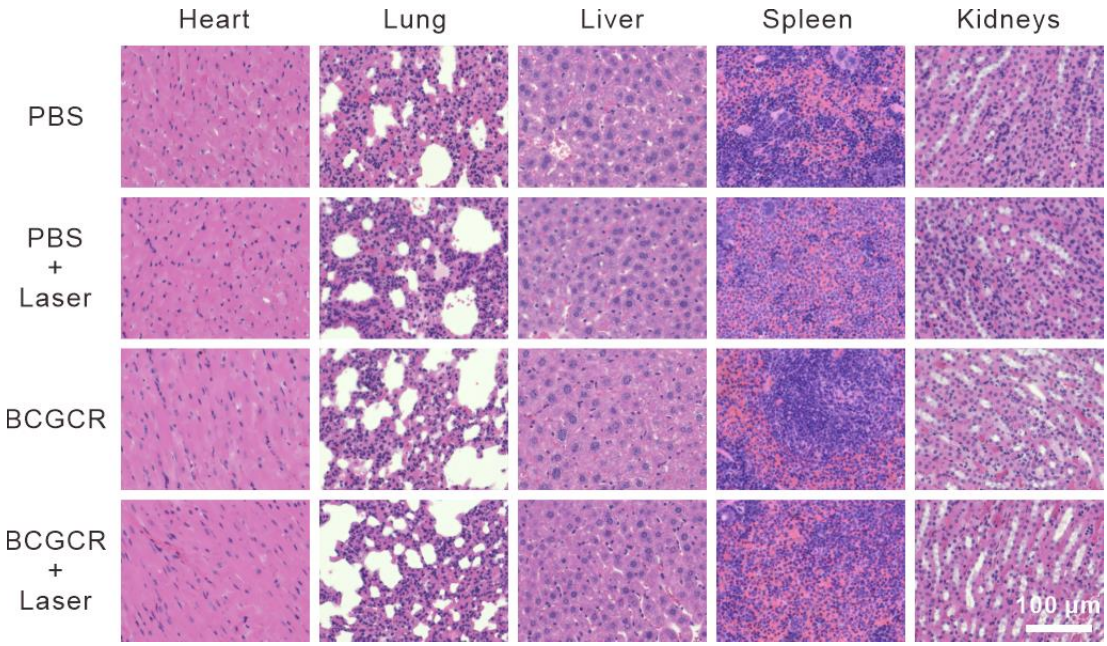

Figure S21. H&E-stained images of major organs including the heart, lungs, liver, spleen and kidneys resected from mice on the 15th day after the indicated treatments.

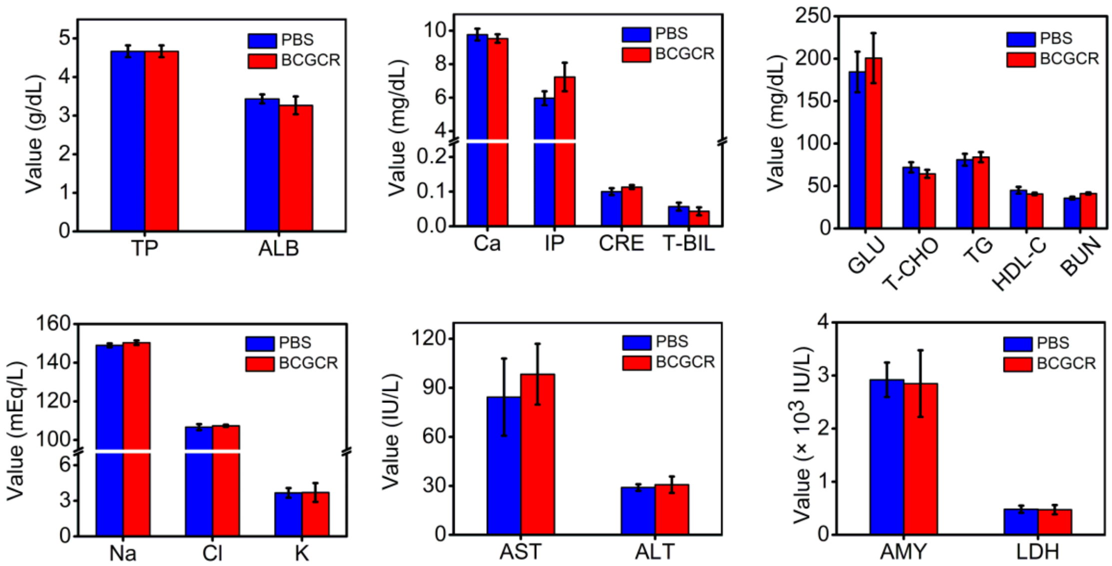

Figure S22. Blood routine examinations of mice at 15 days post-injection of 100 μL PBS or BCGCR (5 mg/kg Cu^{2+}).

TABLES

Table S1. PCE Comparison between reported CuS NPs and BCGCR

CuS NPs	Irradiation wavelength (nm)	PCE (%)	Reference
Gd:CuS@BSA	980	32.3	1
Gd_2O_3/CuS NDs	785	45.5	3
T-MAN	808	70.1	4
PFN	1064	30.17	5
BSA@CuS@DOX	1064	52.81	6
Gd/CuS@PEI-FA-PS	1064	26.7	7
IONF@CuS	1064	42	8
RGD-CuS DENPs	1064	49.8	9
CuSCDs	808	39.7	10
CuS-MnS_2	808	67.5	11
Cu_2MnS_2	1064	49.4	12
HCuS@Cu_2S@Au	808	35	13
BCGCR	**980**	**30.3**	**This work**

Table S2. Comparison of treatment conditions between reported CuS NPs and BCGCR for tumor therapy.

CuS NPs	Therapy	Tumor cell line	Dose (mg/kg)	Irradiation λ[a] (nm)	Irradiation Time (min)	Power density (W/cm^2)	Reference
Gd:CuS@BSA	PTT	SK-OV-3	10	980	5	0.8	1
Gd_2O_3/CuS NDs	PTT	4T1	4.8	785	5	1.5	3
T-MAN	PTT	MKN45	5	808	10	0.8	4
PFN	PTT/CDT	Panc02	20	1064	5	1.0	5
BSA@CuS@DOX	PTT/CT[b]	4T1	3 for DOX	1064	6	1.2	6
Gd/CuS@PEI-FA-PS	PTT	KB-LFAR	~3.5	1064	10	0.6	7
IONF@CuS	MHT[c]/PTT	PC3	~0.32[d]	1064	10	1.0	8
RGD-CuS DENPs	PTT/gene	MDA-MB-231	~1.4	1064	5	0.6	9
CuSCDs	PTT	4T1	5[e]	808	5	0.3	10
CuS-MnS_2	PDT/PTT	A2780	~0.56[d]	808	10	1.0	11
Cu_2MnS_2	PTT	S180	20	1064	10	0.6	12
HCuS@Cu_2S@Au	PTT	U87MG	13	808	5	0.8	13
BCGCR	**PTT/CDT**	**U87MG**	**5**	**980**	**10**	**0.8**	**This work**

[a]λ: wavelength; [b]CT: chemotherapy; [c]MHT: magnetic hyperthermia; [d]i.t. injection; [e]injection every two days.

NOTE S1. PCE Evaluation of BCGCR

PCE (η) is used to evaluate the extent of conversion of absorbed light into temperature increase, which can be calculated according to the method of previous reports[14-16] with the modified formula:

$$\eta = \frac{hS(T_{max,mix} - T_{max,s})}{I(1 - 10^{-A_\lambda})} \times 100\%$$

where h is the heat transfer coefficient; S is the surface area of the cuvette; $T_{max,mix}$ is the maximum temperature of solvent with nanoparticles (54.8°C from Figure S9a), while $T_{max,s}$ is that of solvent alone after irradiation for the same time (31.2°C); I is the laser power ($0.8\ W/cm^2 \times \pi \times (0.5\ cm)^2 = 0.628\ W$); A_λ is the absorbance of nanoparticles at the wavelength λ ($A_{980} = 0.86$). hS can be calculated as follows:

$$hS = \frac{mC_{water}}{\tau_s}$$

$$\tau_s = -\frac{t}{\ln\theta} = -\frac{t}{\ln\frac{T - T_{sur}}{T_{max,mix} - T_{sur}}}$$

where m is the mass of the sample solution (0.3 g); C_{water} is the heat capacity of water (4.2 J g^{-1} K^{-1}); τ_s is the thermal time constant that can be determined as the slope by linear fit of the time point t vs (- Lnθ) during the natural cooling period; T is the temperature at the time point t; T_{sur} is the temperature of the surroundings.

According to Figure S9b, τ_s is calculated as 181.6 s. Hence,

$$hS = \frac{mC_{water}}{\tau_s} = \frac{0.3\ g \times 4.2\ J\ g^{-1}\ K^{-1}}{181.6\ s} = 0.00694\ W\ K^{-1}$$

$$\eta = \frac{hS(T_{max,mix} - T_{max,s})}{I(1 - 10^{-A_\lambda})} \times 100\% = \frac{0.00694\ W\ K^{-1} \times (327.95\ K - 304.35\ K)}{0.628\ W \times (1 - 10^{-0.86})} \times 100\%$$

$$= \frac{0.1638\ W}{0.5413\ W} \times 100\% = 30.3\%$$

REFERENCES

(1) Yang, W.; Guo, W.; Le, W.; Lv, G.; Zhang, F.; Shi, L.; Wang, X.; Wang, J.; Wang, S.; Chang, J.; Zhang, B. Albumin-Bioinspired Gd:CuS Nanotheranostic Agent for In vivo Photoacoustic/Magnetic Resonance Imaging-Guided Tumor-Targeted Photothermal Therapy. *ACS Nano* **2016**, *10*, 10245-10257.

(2) Tang, W.; Gao, H.; Ni, D.; Wang, Q.; Gu, B.; He, X.; Peng, W. Bovine Serum Albumin-templated Nanoplatform for Magnetic Resonance Imaging-Guided Chemodynamic Therapy. *J. Nanobiotechnol.* **2019**, *17*, 68.

(3) Wen, R.; Lv, X.; Yang, T.; Li, Y.; Tang, Y.; Bai, X.; Ke, H.; Shen, J.; Chen, H. Albumin Nanoreactor-templated Synthesis of Gd_2O_3/CuS Hhybrid Nanodots for Cancer Theranostics. *Sci. China Mater.* **2017**, *60*, 554-562.

(4) Shi, H.; Sun, Y.; Yan, R.; Liu, S.; Zhu, L.; Liu, S.; Feng, Y.; Wang, P.; He, J.; Zhou, Z.; Ye, D. Magnetic Semiconductor Gd-Doping CuS Nanoparticles as Activatable Nanoprobes for Bimodal Imaging and Targeted Photothermal Therapy of Gastric Tumors. *Nano Lett.* **2019**, *19*, 937-947.

(5) Sun, H.; Zhang, Y.; Chen, S.; Wang, R.; Chen, Q.; Li, J.; Luo, Y.; Wang, X.; Chen, H. Photothermal Fenton Nanocatalysts for Synergetic Cancer Therapy in the Second Near-Infrared Window. *ACS Appl. Mater. Interfaces* **2020**, *12*, 30145-30154.

(6) Zhu, L.; Gao, D.; Xie, L.; Dai, Y.; Zhao, Q. NIR II-Excited and pH-Responsive Ultrasmall Nanoplatform for Deep Optical Tissue and Drug Delivery Penetration and Effective Cancer Chemophototherapy. *Mol. Pharmaceutics* **2020**, *17*, 3720-3729.

(7) Zhang, C.; Sun, W.; Wang, Y.; Xu, F.; Qu, J.; Xia, J.; Shen, M.; Shi, X. Gd-/CuS-Loaded Functional Nanogels for MR/PA Imaging-Guided Tumor-Targeted Photothermal Therapy. *ACS Appl. Mater. Interfaces* **2020**, *12*, 9107-9117.

(8) Curcio, A.; Silva, A. K. A.; Cabana, S.; Espinosa, A.; Baptiste, B.; Menguy, N.; Wilhelm, C.; Abou-Hassan, A. Iron Oxide Nanoflowers @ CuS Hybrids for Cancer Tri-Therapy: Interplay of Photothermal Therapy, Magnetic Hyperthermia and Photodynamic Therapy. *Theranostics* **2019**, *9*, 1288-1302.

(9) Ouyang, Z.; Li, D.; Xiong, Z.; Song, C.; Gao, Y.; Liu, R.; Shen, N.; Shi, X. Antifouling Dendrimer-Entrapped Copper Sulfide Nanoparticles Enable Photoacoustic Imaging-Guided Targeted Combination Therapy of Tumors and Tumor Metastasis. *ACS Appl. Mater. Interfaces* **2021**, *13*, 6069-6080.

(10) Yu, Y.; Song, M.; Chen, C.; Du, Y.; Li, C.; Han, Y.; Yan, F.; Shi, Z.; Feng, S. Bortezomib-Encapsulated CuS/Carbon Dot Nanocomposites for Enhanced Photothermal Therapy via Stabilization of Polyubiquitinated Substrates in the Proteasomal Degradation Pathway. *ACS Nano* **2020**, *14*, 10688-10703.

(11) Chen, W.; Wang, X.; Zhao, B.; Zhang, R.; Xie, Z.; He, Y.; Chen, A.; Xie, X.; Yao, K.; Zhong, M.; Yuan, M. CuS-MnS_2 Nano-flowers for Magnetic Resonance Imaging Guided Photothermal/Photodynamic Therapy of Ovarian Cancer Through Necroptosis. *Nanoscale* **2019**, *11*, 12983.

(12) Ke, K.; Yang, W.; Xie, X.; Liu, R.; Wang, L. L.; Lin, W. W.; Huang, G.; Lu, C. H.; Yang, H. H. Copper Manganese Sulfide Nanoplates: A New Two-Dimensional Theranostic Nanoplatform for MRI/MSOT Dual-Modal Imaging-Guided

Photothermal Therapy in the Second Near-Infrared Window. *Theranostics* **2017**, *7*, 4763-4776.

(13) Deng, X.; Li, K.; Cai, X.; Liu, B.; Wei, Y.; Deng, K.; Xie, Z.; Wu, Z.; Ma, P.; Hou, Z. A Hollow-Structured $CuS@Cu_2S@Au$ Nanohybrid: Synergistically Enhanced Photothermal Efficiency and Photoswitchable Targeting Effect for Cancer Theranostics. *Adv. Mater.* **2017**, *29*, 1701266.

(14) Younis, M. R.; Wang, C.; An, R.; Wang, S.; Younis, M. A.; Liu, Z.; Wang, Y.; Ihsan, A.; Ye, D.; Xia, X. Low Power Single Laser Activated Synergistic Cancer Phototherapy Using Photosensitizer Functionalized Dual Plasmonic Photothermal Nanoagents. *ACS Nano* **2019**, *13*, 2544-2557.

(15) Ren, W.; Yan, Y.; Zeng, L.; Shi, Z.; Gong, A.; Schaaf, P.; Wang, D.; Zhao, J.; Zou, B.; Yu, H.; Chen, G.; Brown, E. M. B.; Wu, A. A Near Infrared Light Triggered Hydrogenated Black TiO_2 for Cancer Photothermal Therapy. *Adv. Healthcare Mater.* **2015**, *4*, 1526-1536.

(16) Liu, Y.; Ai, K.; Liu, J.; Deng, M.; He, Y.; Lu, L. Dopamine-Melanin Colloidal Nanospheres: An Efficient Near-Infrared Photothermal Therapeutic Agent for In vivo Cancer Therapy. *Adv. Mater.* **2013**, *25*, 1353-1359.